Three-dimensional phase imaging with a scanning optical-fiber interferometer

Julian N. Walford, Keith A. Nugent, Ann Roberts, and Robert E. Scholten

We describe a quantitative method for measuring the phase of a propagating wave field in three dimensions by use of a scanning optical-fiber interferometer. Because phase modulation in the reference arm is exploited, this technique is insensitive to large variations in the intensity of the field being studied and is therefore highly suitable for measurement of phase within spatially confined optical beams. It uses only a single detector and is not reliant on lock-in electronics. The technique is applied to the measurement of the near field of a cleaved optical fiber and is shown to produce results in good agreement with theory. © 1999 Optical Society of America

OCIS codes: 060.2300, 060.5060, 120.3180, 120.5050, 180.3170, 180.5810.

1. Introduction

We describe the development of a high-resolution quantitative optical-phase microscope based on a scanning fiber interferometer. Interferometric techniques are of great general interest, for example, in the characterization of surfaces, the measurement of vibrations, and the measurement of physical properties such as temperature and pressure.[1,2]

In addition to the measurement of the properties of physical objects, interferometric techniques can be used to study the distribution of phase within propagating wave fields. In particular, there are many optical wave fields that possess interesting phase discontinuities and dislocations. These include the field near the focus of a lens (the Gouy phase anomaly) and the so-called donut beams (optical vortices). As well as having optical fields that possess unusual phase behavior, it is also important to be able to characterize the near-field phase distribution of optical waveguiding devices. For example, in fiber–fiber splicing and other fiber-coupling operations, it is commonly held that optimal coupling is obtained when the intensity distributions of the two modes coincide; in fact, optimal coupling is obtained when phase distributions also match exactly.[3] Also, a number of integrated optical components, such as multimode interference (MMI) splitters, rely on the control of the phase relation between individual waveguides. MMI splitters exhibit self-imaging properties, which make them useful for wavelength division multiplexing. The operation of multiplexers is determined by the relation between the phases of various inputs into a star coupler; therefore knowledge of these relations is central to the development of such devices.[4]

Measurements of the near-field phase of MMI splitters and of laser arrays have previously been performed in a shearing Sagnac interferometer[5,6]; however, shearing Sagnac interferometers rely on the reimaging of the near field by propagation through a lens system or free space, and this propagation imposes a resolution limit of the order of a wavelength. Iiyama *et al.*[7] have obtained optical intensity and phase maps by scanning a tapered fiber probe through the field emitted from an optical fiber and have produced an interference pattern by illuminating a screen with light emitted from probe and reference fibers. The introduction of a mask at the detector stage allowed the determination of a quantitative phase map from this interferogram.[8] The mask was aligned with the fringes and had to be physically scanned across the detector plane simultaneously with the scanning of the probe through the field.

We present here a fully fiber-based technique in which fiber directional couplers are used. This technique permits quantitative measurement of the phase of an optical field with a single detector and by

The authors are with the School of Physics, University of Melbourne, Parkville 3052, Australia. A. Roberts e-mail address is a.roberts@physics.unimelb.edu.au.

Received 17 September 1998; revised manuscript received 10 March 1999.

0003-6935/99/163508-08$15.00/0

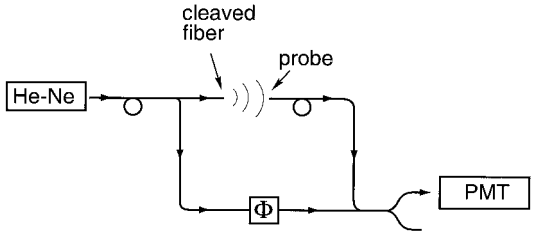

Fig. 1. Schematic of device, including He–Ne laser, phase modulator Φ, and photomultiplier tube PMT.

means of sequential measurements of a phase-modulated signal.

Our technique uses a Mach–Zehnder fiber interferometer similar to those in fiber-optic sensing applications.[9,10] However, in our apparatus, the fiber in one arm of the interferometer is broken to allow light to propagate in free space, and phase and amplitude maps of this field are measured in three dimensions.

The primary advantages of this technique are its speed, its accounting for modulator hysteresis and nonlinearity, and its ability to produce a simultaneous measurement of the intensities in the two arms of the interferometer. One achieves high speed by performing only rapid data sampling during the scanning procedure and by separate calculation of a phase map. Unlike Fourier techniques such as that of Takeda *et al.*,[11] our technique also provides a simultaneous measurement of phase and intensity at each scan point, independent of the broad structure of the scanned image.

2. Quantitative Phase Measurement within a Scanning Fiber Interferometer

Figure 1 shows a schematic of the experimental apparatus. A He–Ne laser is used as a light source. This is launched into a single-mode optical fiber, which is split into two arms: the signal and the reference. The fiber in the signal arm is cleaved to produce a freely propagating beam. A probe fiber is positioned in the beam close to the cleaved end face of the source fiber. Scanning the probe through this field records an image of the source near field. The field that couples into the probe fiber is superimposed with the mode propagating through the reference arm via a fiber coupler, producing an interference signal in both fibers. Only one of these is recorded, by use of a photomultiplier tube. A phase modulator in the reference arm allows for variation of the phase difference between arms. In this section we discuss the technique employed to measure a quantitative phase difference at each point in the probe scan.

A. Theoretical Basis

Assuming perfect mixing, we will observe

$$I = \frac{1}{2}[I_S + I_R + 2(I_S I_R)^{1/2} \cos \delta], \qquad (1)$$

if half the power in each fiber is coupled into the other, where I_S and I_R are the intensity of the modes entering the coupler from the signal and the reference arms, respectively, and δ is the phase difference between the two arms. Some techniques to measure phase involve measurements of both outputs of an interferometer,[12] but these share a common difficulty in obtaining an accurate calibration of two detectors relative to each other, particularly when the intensity in one arm may vary significantly between consecutive phase measurements. Our technique measures phase and uses only one output, avoiding the need for balancing two separate detectors. This use of only one detector to calculate the phase is achieved by measuring the interference signal synchronously with a phase variation introduced in the reference arm by a phase modulator.

Several phase measurement schemes based on phase modulation exist. Both homodyne and heterodyne techniques are used to measure phase in Mach–Zehnder fiber interferometers. With a sinusoidal modulation applied to the measured phase signal, active stabilization can be used to lock the interferometer output to a zero crossing,[13] allowing one to measure either the amplitude of the oscillating phase signal (dynamic phase[14]) or the magnitude of the correction phase applied to maintain the system in quadrature (static phase[15,16]). Within the scope of the experiment considered in this paper, we are not interested in the amplitude or the depth of the dynamic phase modulation, and we avoid schemes that are based on feedback locking of the interferometer to a zero crossing. Although these provide a highly sensitive measure of the static phase difference between arms, they provide no direct means of determining the intensity of the two signals being interfered, whereas the signal intensity is of interest in a microscopy application.

A further difficulty present in lock-in techniques is the time taken to lock on to the oscillating signal. As a separate phase measurement is recorded at each pixel in a scan (necessary to maintain good spatial resolution), the time taken to lock on to the signal at each step would make a lock-in system intolerably slow.

The modulation employed here is of the pseudoheterodyne type, with a linear ramping function applied to the phase modulator at each point of phase measurement. The detection and measurement of phase is carried out analytically on a series of discretely sampled and digitized points through the modulation cycle. The curve-fitting procedure outlined below involves taking a product of the sampled data with a periodic function representing the modulation signal. The term digital heterodyne is frequently applied to this form of interferometry.[17,18]

Equation (1) ignores any loss of visibility from imperfect mixing at the second coupler due to, for example, polarization variations in the two arms. Provided instability in polarization does not vary on the time scale needed to measure the phase at any point, there will be no effect on the phase measured

by a heterodyne interferometer. The simultaneously calculated intensity images are affected by this variation in visibility, and thus these may not be quantitatively reliable if the polarization varies during a single scan. We believe that if one carefully controls the environment of the interferometer, any variations in signal visibility occur over time scales longer than an entire scan, and so valid intensity images can be obtained with a suitable determination of a visibility factor. Consequently, no attempt has been made to control polarization.

Changes in the phase difference between the two arms then come from two sources. The movement of the probe through the field produces a phase shift that corresponds to the spatial variation of phase, and it is this phase, $\phi_{\text{probe}}(x, y)$, that we wish to measure at each point in the scan. The phase modulator in the reference arm also causes a phase change of $\phi_{\text{mod}}(t)$, which varies continually with time. The probe scan is performed stepwise, with data acquisition triggered at each step, allowing phase measurements to be performed point by point. The probe position is thus considered to be time independent. Our experiment measures

$$I(x, y, t) = I_S(x, y) + I_R + 2[I_S(x, y)I_R]^{1/2} \cos[\delta(x, y, t)], \quad (2)$$

where

$$\delta(x, y, t) = \phi_{\text{probe}}(x, y) + \phi_{\text{mod}}(t). \quad (3)$$

The goal of our experiment is to determine $\phi_{\text{probe}}(x, y)$ and the signal intensity map $I_S(x, y)$, and to do this, ϕ_{mod} must be known.

The phase response of the modulator to a driving voltage V is

$$\phi_{\text{mod}}(V) = [f(V(t)]. \quad (4)$$

The function f is determined by a calibration procedure (Subsection 2.B).

At each scan point (x, y), a series of N measurements of the intensity $I_j (j = 1, \ldots N)$ are recorded:

$$I_j(x, y) = I_S(x, y) + I_R + 2[I_S(x, y)I_R]^{1/2} \times \cos[\phi_{\text{probe}}(x, y) + \phi_j], \quad (5)$$

where $\phi_j \equiv \phi_{\text{mod}}(V_j) = f(V_j)$.

Algebraic inversion of Eq. (5) is possible with $N = 3$, through solution of three simultaneous equations for the variables I_S, I_R, and ϕ_{probe}.[19] Such an inversion is highly sensitive to noise. Although averaging over a number of measurements for each distinct value of $\phi_{\text{mod}}(V_j)$ reduces this noise, the time required for the phase modulator to reach a fixed and stable value of ϕ_{mod} after a step change in V would prohibitively increase the data-collection time.

The phase modulator is driven by a sinusoidally varying voltage $V = V_0 \sin(\omega t) + V_{\text{dc}}$ so that ϕ_{mod} varies smoothly and continuously. Data acquisition is gated to occur only during the approximately linear part of the cycle, simulating a sawtooth waveform. A series of interference samples is taken at distinct ϕ_j during this modulation cycle.

A least-squares fit is used to find the values of I_R, I_S, and ϕ_{probe} that minimize the deviation of the curve $I(V)$ from the measured data.[18] This also has the effect of data smoothing.

Rather than using an iterative curve-fitting procedure, we reformulate Eq. (5) so that it becomes linear in some combination of the parameters. This is done by use of trigonometric identities to rearrange Eq. (2) as

$$I = A + B \cos[\phi_{\text{mod}}(V)] + C \sin[\phi_{\text{mod}}(V)] \quad (6)$$

with new variables

$$A \equiv I_S + I_R,$$
$$B \equiv 2(I_S I_R)^{1/2} \cos(\phi_{\text{probe}}),$$
$$C \equiv 2(I_S I_R)^{1/2} \sin(\phi_{\text{probe}}). \quad (7)$$

The condition to minimize the sum of the squares is expressed as a matrix equation:

$$\begin{bmatrix} \sum \sin^2(\phi_j) & \sum \sin(\phi_j)\cos(\phi_j) & \sum \sin(\phi_j) \\ \sum \sin(\phi_j)\cos(\phi_j) & \sum \cos^2(\phi_j) & \sum \cos(\phi_j) \\ \sum \sin(\phi_j) & \sum \cos(\phi_j) & N \end{bmatrix} \times \begin{bmatrix} A \\ B \\ C \end{bmatrix} = \begin{bmatrix} \sum y_j \sin(\phi_j) \\ \sum y_j \cos(\phi_j) \\ \sum y_j \end{bmatrix}, \quad (8)$$

which is solved by inversion for A, B, and C. Each element of this array that is subscripted by j is summed over the number of data points, N, which was typically 10 in our experiments.

Equations (7) are inverted to find I_S and I_R. Because the parameters A, B, and C are symmetrically dependent on I_S and I_R, these intensities are indistinguishable in the inversion. Hence rather than calculating I_S and I_R, we determine two intensities I_+ and I_-:

$$I_{\pm} = \frac{A \pm (A^2 - B^2 - C^2)^{1/2}}{2}, \quad (9)$$

where I_+ is the larger of the two solutions.

One of these is the intensity coming through the probe in the signal arm; the other is the intensity of the reference mode. There is no absolute method to distinguish between these two variables to determine which corresponds to the signal intensity and which to the reference intensity, and we therefore must rely on some other information to make this identification. For example, the signal intensity measurements are correlated with the raster scan of the probe in space, whereas the reference intensity remains more or less constant throughout the scan. This permits identification of either I_+ or I_- with the signal intensity I_S.

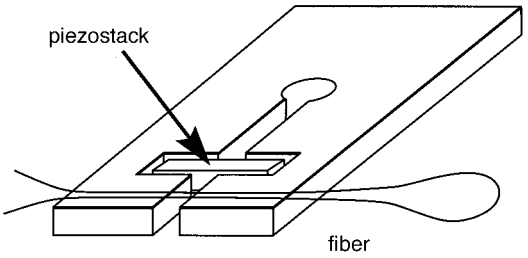

Fig. 2. Design for fiber phase modulator driven by a piezostack, capable of imparting a phase shift of 8π rad with a driving voltage of amplitude 40 V.

B. Phase Modulator: Design and Calibration

The modulation of the phase difference between the two arms allows the separation of intensity and phase as described above. Several techniques can be used to produce a phase modulation in an optical fiber, including the wrapping of an optical fiber around a piezoceramic tube that expands radially,[20] the attachment of the fiber to a piezofilm to impart a longitudinal strain,[21] and the application of a piezoceramic coating to a fiber to stimulate radial acoustic modes.[22] We found that the first method introduces bending strains that increase coupling between core and cladding modes and hence coupling of the propagating mode to the external environment, leading to large signal instabilities. Piezofilms were too slow for our requirements. Acousto-optic phase modulators are not readily available for specialized fiber and are difficult to construct.

The modulator we have developed (Fig. 2) has a simple construction, keeps the fiber relatively straight and free from bending strains, and achieves a phase-modulation rate of approximately 5 krad/s. A fiber is bonded in two passes over a split metal sheet, which is strained by a piezoelectric stack (Tokin AE0203D08) inserted at the split. This acts like a tuning fork, responding in an approximately linear manner to a sinusoidal driving voltage at the tuning resonance of approximately 200 Hz. This operating frequency was chosen to match probe scanning and data-acquisition rates. The phase change imparted on the fiber is approximately 8π with a driving voltage of under 40 V.

A calibration function relating the imparted phase shift to the driving voltage is necessary to be able to evaluate the parameters of best fit. For evaluating the phase response function $f(V)$ in Eq. (4), the position of the probe is held fixed so that the unknown parameters I_S, I_R, and ϕ_{probe} are all constant. Then Eq. (2) becomes

$$I_j = a' + b' \cos[c' + f(V_j)], \tag{10}$$

and it is possible to determine a suitable approximation for $f(V)$ by means of the assumption that the response can be approximated as a low-order polynomial series in V_j:

$$f(V_j) = a_0 + a_1 V_j + a_2 V_j^2 + a_3 V_j^3. \tag{11}$$

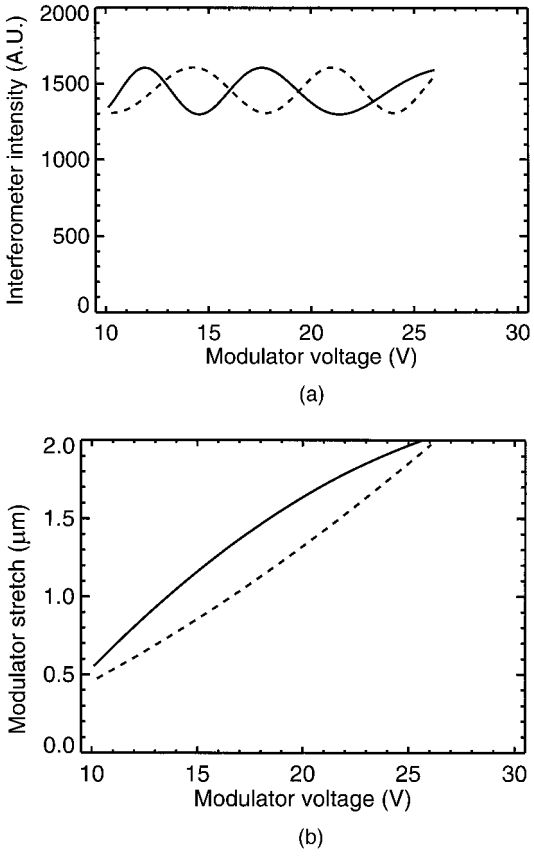

Fig. 3. (a) Interferogram obtained when the phase modulator in the reference arm is operated. The interferometric signal is plotted versus the driving voltage applied to the phase modulator. The dashed curve represents that part of the signal recorded whilst the fiber is being strained (increasing modulator voltage/piezoexpansion), and the solid curve is the interferogram recorded whilst the fiber is being relaxed (decreasing modulator voltage/piezocontraction). (b) Phase (or fiber elongation) imparted by phase modulator, calculated through a polynomial sine fit to the interferogram shown in (a).

A least-squares fit to an extremely large number of V_j determines the a_i that best describes the curve. In practice, there is a phase lag between the driving signal and the response of the modulator, with some degree of hysteresis. Figure 3 shows a typical interferogram represented by Eq. (10) and the calculated phase response with the quadratic fit in Eq. (11). This low-order nonlinear approximation for the phase response function is not accurate near the turning points of the driving voltage signal and is multivalued elsewhere. Synchronization of the detection system with this driving signal is therefore necessary to limit the range of the modulation during which data is recorded to the approximately linear region where the driving signal is increasing in magnitude and thus produces the pseudoheterodyne modulation described above. A calibration interferogram and the corresponding phase response curve for this windowed region are shown in Fig. 4.

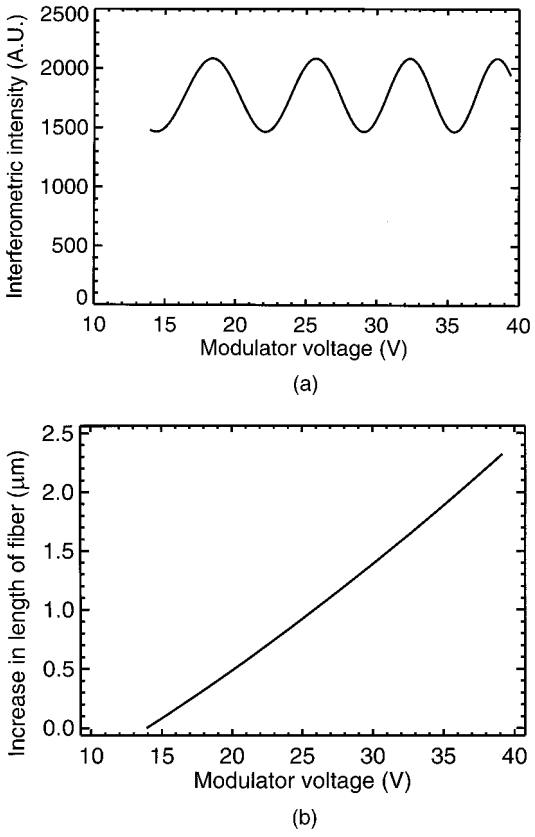

Fig. 4. (a) Interferogram and (b) calibration curve obtained when the data-acquisition time about the increasing part of the driving voltage signal only is windowed.

C. Implementation

Light from a He–Ne laser operating at 632.8 nm was coupled into a single-mode fiber, and passed through a 90/10 directional fused-fiber coupler. The fiber with the greater intensity was used for the signal arm, as only a very small fraction of the freely propagating light field is coupled back into the signal arm.

This signal arm fiber was connected to a cleaved optical fiber polished at an angle of 7° to minimize unwanted reflections. A fiber cleaved perpendicular to its optical axis was used as a probe for the field emitted from the angled fiber tip. The fiber probe was connected to the reference fiber through a 50/50 directional fused-fiber coupler, which provides maximum contrast through the largest range of possible signal intensities. The reference fiber was bonded to the phase modulator, as described above. One of the fiber outputs from the final 50/50 coupler was passed to a photomultiplier tube connected to an analog-to-digital converter input on a computer, which simultaneously controlled the scanning of the probe. The phase modulator was driven by a function generator at 200 Hz, and the data acquisition was gated and synchronized with this driving signal.

Throughout the system, fibers were taped to the optical bench to reduce both mechanical and thermal fluctuations in the signal. The entire apparatus was in an enclosed environment to reduce thermal drifts further.

The probe scanning apparatus consisted of a hollow piezoelectric transducer piezoceramic tube, coated with nickel segmented into quadrants. The probe was positioned on the axis of the tube, and its scanning motion calibrated with a Michelson interferometer.

3. Results

The scanning interferometer was used in this configuration to map the near field of the cleaved single-mode optical fiber. This field is well understood theoretically. Quantitative measurement of the radius of curvature of the beam at different distances from its waist provides a confirmation of the accuracy of our phase measurement technique.

A. Theoretical Predictions

The field at the end face of an optical fiber is approximately Gaussian in cross section,[3] the approximation becoming exact for a parabolic index profile. This approximation has been validated with near-field intensity measurements.[23] We use a Gaussian-beam model to represent the far-field distribution.

The waist of the beam is at the fiber end face, and its diameter is equal to the mode-field diameter. The fiber used had a mode-field diameter of 3.92 μm at 630 nm. Gaussian-beam theory predicts that the electric field E is given by

$$E(r, z) = E(0, 0)\,\frac{\omega_0}{\omega(z)}\exp\left[\frac{-r^2}{\omega^2(z)}\right] \times \exp\left\{-i\left[kz - \Phi(z) + \frac{kr^2}{2R(z)}\right]\right\}, \quad (12)$$

where the beam is assumed to be propagating in the positive z direction. The beam radius is ω, equal to ω_0 at the waist; the radius of curvature of the beam is R; the radial position variable (distance from optic axis of beam) is r; and the Gouy phase shift is Φ. The parameter z_0 is the Rayleigh length, the characteristic length over which the beam broadens as it propagates.

The phase component of the Gaussian field has three components. The first, kz, is the phase advance along the optical axis that would be expected for an infinite plane wave of wavelength λ. The Gouy phase shift $\Phi(z)$ varies monotonically from 0 to $\pi/2$, from the waist to a point distant from the fiber. This is the phase deviation of a Gaussian beam from a plane wave. The last term is a radial parabolic curvature whose radius of curvature varies with distance along the optical axis. We measured this component of the phase distribution at a range of distances from the beam waist.

B. Results for Gaussian Beam

Images of the phase (modulo 2π) through a plane containing the optical axis of the beam emitted from the polished fiber tip are shown in Fig. 5. Figure

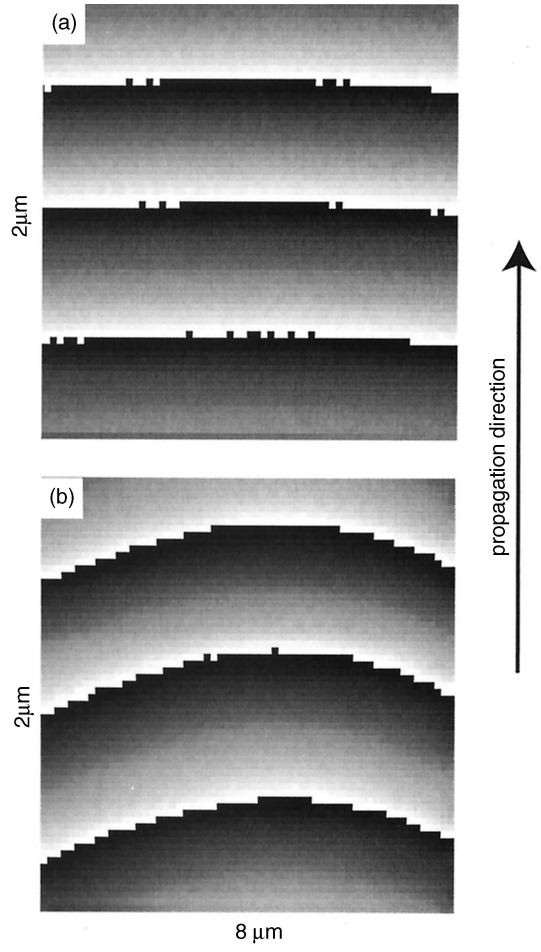

Fig. 5. Two phase maps of a Gaussian beam recorded at different distances from the beam waist, by the probe scanning in a plane, including the beam axis. The beam is propagating upward in the images. The images are approximately 8 μm across and 2 μm along the optical axis direction (vertical axis in the image). The gray scale represents the phase of the beam wrapped into the 0-to-2π range. (a) Image recorded at a very large distance from the waist, where the radius of curvature is large. (b) Image recorded at approximately the Rayleigh length from the waist, where the radius of curvature is minimum.

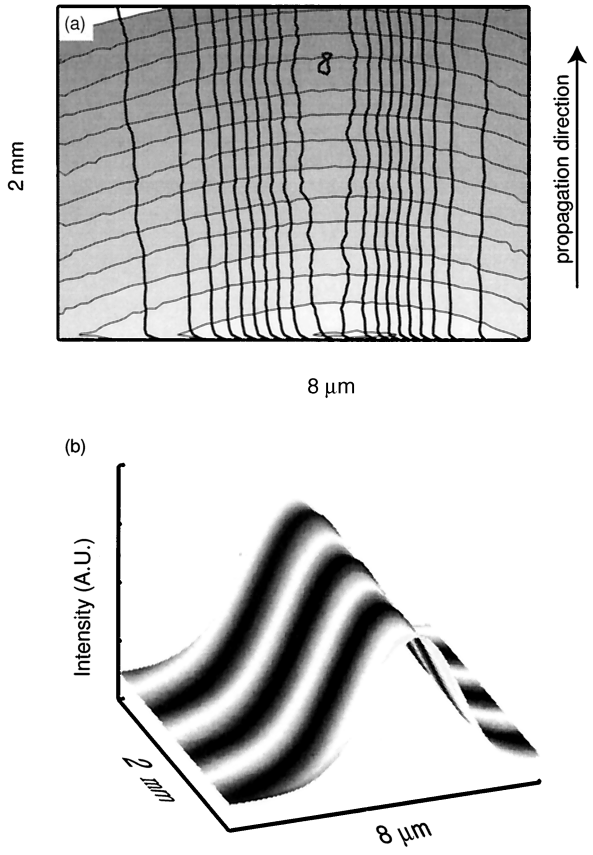

Fig. 6. Two images showing the superposition of intensity data with phase data. (a) Contour plot of intensity (hollow contours) superimposed over a contour plot of phase (shaded regions). (b) Isometric plot of the field, with shading representing the cosine of the phase and the height of the surface representing beam intensity.

5(a) shows the phase wrapped into the 0-to-2π range a large distance from the beam waist where the beam is approximately planar over the scan region. Figure 5(b) shows the phase at approximately the Rayleigh length from the fiber tip, where the radius of curvature is smallest. The phase resolution in these plots is calculated by consideration of the uncertainties in the fit parameters that are used to calculate phase. This phase resolution depends point by point on a number of factors, including the contrast at each point. Higher phase errors obviously exist in regions of poor fringe contrast (where the signal intensity is low). A modest estimate of the phase resolution at the Rayleigh length is 0.05 rad, although this figure varies considerably across the image. This resolution is limited by the short time available for point-by-point data sampling. Much higher phase resolutions are obtainable in phase-locked homodyne systems, but these are restricted in both sampling speed and ability to produce a concurrent intensity image.

The fringe contrast vanishes almost entirely where the intensity is very low, that is, at the edges of these scans. However, the recovered phase image is both continuous and plausible in these regions. A strength of this technique is its ability to produce continuous quantitative phase maps without artifacts due to large intensity variations across the field.

The intensity image at the Rayleigh length is shown as hollow contours, overlaid on the (unwrapped) phase in Fig. 6(a), and in isometric form with the phase structure superimposed as shading in Fig. 6(b). This intensity image is calculated from the same data that produced the phase maps, ensuring an absolute registration between pixels in the two images.

C. Comparison of Experiment with Theory

The curves marking the 2π phase discontinuities that result from wrapping of the recovered phase images reveal the general form of the lines of constant phase in this region of the field. A slice through this image in a line at a constant distance from the beam waist shows the phase to follow a quadratic curve, as ex-

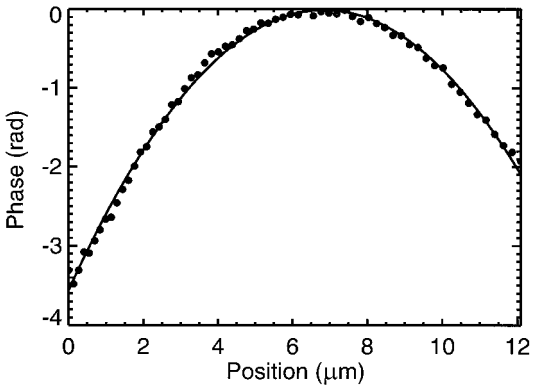

Fig. 7. Slice through the phase image showing the data to match the expected quadratic form. The solid curve is a least-squares fit.

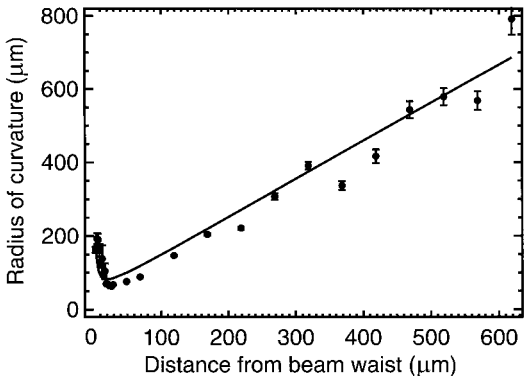

Fig. 8. Radius of curvature measured at different distances from the fiber waist (discrete points) and with a fit based on the theoretical form of the radius of curvature. Error bars represent the error in the quadratic coefficient.

pected (Fig. 7). The solid curve in Fig. 7 is a quadratic line of best fit through the data.

The constant term in this fit is an arbitrary additive offset, the quadratic term is directly related to the radius of curvature, and the linear coefficient represents either a tilt in the beam or a displacement between the center of the beam and the zero of our coordinate system.

Equating the quadratic term to a radius of curvature gives us

$$R = \frac{-\pi}{\lambda a_2}. \tag{13}$$

Taking a series of images at different distances from the optical fiber source, we can calculate the radius of curvature with this quadratic fit and thus look at how the radius of curvature changes with distance. Gaussian-beam theory predicts

$$R(z) = z\left[1 + \left(\frac{z_0}{z}\right)^2\right]. \tag{14}$$

We have no independent method for determining the distance of the probe fiber from the source fiber. This distance is determined by a study of the radius of curvature. We expect the radius of curvature to approach infinity as we approach the beam waist ($R \to 1/z$ as $z \to 0$). Using a nonlinear least-squares fit to this data unambiguously determines the location of the asymptote and hence the beam waist.

Figure 8 shows how the experimental data compare with a theoretical fit. The data has been fitted so that the asymptote position coincides with $z = 0$, whereas the calculated Rayleigh length $z_0 \approx 19$ μm (distance from asymptote to minimum) is not permitted to vary during the fit. The essential features of the Gaussian-beam curvature are clearly measured by our interferometer, namely, the asymptotic behavior within the Rayleigh length and the linear behavior beyond this clearly defined point.

4. Conclusions

We have described a new method for phase imaging of optical fields by use of a Mach–Zehnder fiber interferometer with a phase modulator. The digital heterodyne phase measurement technique described has been applied to the construction of a very high resolution scanning optical interferometer. This device has been used for the study of the near field of a single-mode optical fiber, where the field is tightly confined. Our measurement of phase has been confirmed to be quantitatively accurate by measurement of the curvature of the well-understood Gaussian beam.

This technique does not rely on correlation between a number of detectors or on lock-in electronics; thus it is fast and accurate. By means of a calibration procedure, nonlinearity and hysteresis in the modulation is directly accounted for in the phase measurement. This interferometer is particularly useful in the study of regions where the phase variation is of a significantly lower spatial frequency than the intensity variation as described here, allowing the possibility of phase studies in tightly focused fields.

Introduction of a probe with a smaller (subwavelength) diameter aperture allows this technique also to be applied to the study of fields with extremely high spatial frequency phase variations (e.g., fields with phase singularities). Such probes are routinely fabricated for use in the area of near-field microscopy.[24] There is also potential for direct measurement of the near-field phase relations in waveguiding devices such as MMIs in which cutback techniques are used to probe the phase within the couplers.

We gratefully acknowledge the support of the Australian Research Council, and J. N. Walford gratefully acknowledges the support of an Ernst and Grace Matthaei scholarship.

References

1. W. H. Steel, *Interferometry*, 2nd ed. (Cambridge U Press, Cambridge, UK, 1983).

2. M. Born and E. Wolf, *Principles of Optics*, 6th ed. (Pergamon, Oxford, UK, 1980).
3. E. G. Newman, *Single-Mode Fibers* (Fundamentals) (Springer-Verlag, Berlin, 1988).
4. M. Bachmann, P. A. Besse, and H. Melchior, "General self-imaging properties in $N \times N$ multimode interference couplers including phase relations," Appl. Opt. **33,** 3905–3911 (1994).
5. S. Kareenahalli, M. Dagenais, D. Stone, and T. J. Tayag, "Experimental confirmation of phase relationships of multimode interference splitters using a shearing-type Sagnac interferometer," IEEE Photonics Technol. Lett. **9,** 937–939 (1997).
6. C.-P. Cherng, T. C. Salvi, M. Osiński, and J. McInerney, "Near field wavefront measurements of semiconductor laser arrays by shearing interferometry," Appl. Opt. **29,** 2701–2706 (1990).
7. M. Iiyama, T. Kamiya, and H. Yanai, "Optical field mapping using single-mode optical fibers," Appl. Opt. **17,** 1965–1971 (1978).
8. M. Iiyama, T. Kamiya, and H. Yanai, "Automated optical field mapping using a single-mode fiber interferometer," Appl. Opt. **20,** 4296–4301 (1981).
9. C. D. Butter and G. B. Hocker, "Fiber optics strain gauge," Appl. Opt. **17,** 2867–2869 (1978).
10. G. B. Hocker, "Fiber-optic sensing of pressure and temperature," Appl. Opt. **18,** 1445–1448 (1979).
11. M. Takeda and Z. Tung, "Subfringe holographic interferometry by computer-based spatial-carrier fringe-pattern analysis," J. Opt. **16,** 127–131 (1985); T. Kreis, "Digital holographic interference-phase measurement using the Fourier-transform method," J. Opt. Soc. Am. A **3,** 847–855 (1986).
12. For example, D. A. Jackson, A. D. Kersey, M. Corke, and J. D. C. Jones, "Pseudoheterodyne detection scheme for optical interferometers," Electron. Lett. **18,** 1081–1083 (1982).
13. D. A. Jackson, R. Priest, A. Dandridge, and A. B. Tveten, "Elimination of drift in a single-mode optical fiber interferometer using a piezoelectrically stretched coiled optical fiber," Appl. Opt. **19,** 2926–2929 (1980).
14. V. S. Sudarshanam and K. Srinivasan, "Linear readout of dynamic phase change in a fiber-optic homodyne interferometer," Opt. Lett. **14,** 140–142 (1989).
15. V. S. Sudarshanam and K. Srinivasan, "Static phase change in a fiber optic coil hydrophone," Appl. Opt. **29,** 855–863 (1990).
16. V. S. Sudarshanam, "Direct static strain measurement utilizing signal fading and spectrum analysis in a fiber optic interferometric sensor," J. Mod. Opt. **41,** 683–694 (1994).
17. K. Freischlad and C. L. Koliopoulos, "Fourier description of digital phase-measuring interferometry," J. Opt. Soc. Am. A **7,** 542–551 (1990).
18. J. E. Greivenkamp, "Generalized data reduction for heterodyne interferometry," Opt. Eng. **23,** 350–352 (1984).
19. J. C. Wyant, "Use of an ac heterodyne lateral shear interferometer with real-time wave-front correction systems," Appl. Opt. **14,** 2622–2626 (1975).
20. G. Martini, "Analysis of a single-mode optical fiber piezoceramic phase modulator," J. Quant. Elect. **19,** 179–190 (1987).
21. V. S. Sudarshanam and S. B. Desu, "Fiber-optic polarization and phase modulator utilizing transparent piezofilm with indium tin oxide electrodes," Appl. Opt. **34,** 1177–1189 (1995).
22. S. A. Kingsley, "Optical-fiber phase modulator," Electron. Lett. **11,** 453–454 (1975).
23. D. J. Butler, K. A. Nugent, and A. Roberts, "Characterization of optical fibers using near-field scanning optical microscopy," J. Appl. Phys. **75,** 2753–2756 (1994).
24. E. Betzig and J. K. Trautman, "Near-field optics: microscopy, spectroscopy and surface modification beyond the diffraction limit," Science **257,** 189–195 (1992).